Brønsted basicity of the air–water interface

Himanshu Mishra[a,b,c], Shinichi Enami[d,e,f], Robert J. Nielsen[c], Logan A. Stewart[g], Michael R. Hoffmann[a], William A. Goddard III[b,c], and Agustín J. Colussi[a,1]

[a]Ronald and Maxine Linde Center for Global Environmental Science, [b]Materials Science Department, and [c]Materials and Process Simulation Center, California Institute of Technology, Pasadena, CA 91125; [d]The Hakubi Center for Advanced Research, Kyoto University, Kyoto 606-8302, Japan; [e]Research Institute for Sustainable Humanosphere, Kyoto University, Uji 611-0011, Japan; [f]Precursory Research for Embryonic Science and Technology, Japan Science and Technology Agency, Kawaguchi 332-0012, Japan; and [g]Physics Department, University of California, Santa Barbara, Santa Barbara, CA 93106

Edited by Michael L. Klein, Temple University, Philadelphia, PA, and approved October 2, 2012 (received for review June 1, 2012)

Differences in the extent of protonation of functional groups lying on either side of water–hydrophobe interfaces are deemed essential to enzymatic catalysis, molecular recognition, bioenergetic transduction, and atmospheric aerosol–gas exchanges. The sign and range of such differences, however, remain conjectural. Herein we report experiments showing that gaseous carboxylic acids RCOOH(g) begin to deprotonate on the surface of water significantly more acidic than that supporting the dissociation of dissolved acids RCOOH(aq). Thermodynamic analysis indicates that > 6 H_2O molecules must participate in the deprotonation of RCOOH(g) on water, but quantum mechanical calculations on a model air–water interface predict that such event is hindered by a significant kinetic barrier unless OH^- ions are present therein. Thus, by detecting $RCOO^-$ we demonstrate the presence of OH^- on the aerial side of on pH > 2 water exposed to RCOOH(g). Furthermore, because in similar experiments the base $(Me)_3N$(g) is protonated only on pH < 4 water, we infer that the outer surface of water is Brønsted neutral at pH ∼3 (rather than at pH 7 as bulk water), a value that matches the isoelectric point of bubbles and oil droplets in independent electrophoretic experiments. The OH^- densities sensed by RCOOH(g) on the aerial surface of water, however, are considerably smaller than those at the (>1 nm) deeper shear planes probed in electrophoresis, thereby implying the existence of OH^- gradients in the interfacial region. This fact could account for the weak OH^- signals detected by surface-specific spectroscopies.

gas–liquid reactions | surface potential | water surface acidity | interfacial proton transfer

Acid–base chemistry at aqueous interfaces lies at the heart of major processes in chemistry and biology. Changes in the degree of dissociation of the acidic/basic residues upon translocation between aqueous and hydrophobic microenvironments orchestrate enzyme catalysis (1), drive proton/electron transport across biomembranes (2, 3), and mediate molecular recognition and self-assembly phenomena (4–6). Despite its importance, the characterization of acid–base chemistry at aqueous interfaces remains fraught with uncertainties (7–11). Basic questions linger about the thickness of interfacial layers (12), how acidity changes through the interfacial region (13), and the mechanistic differences between proton transfer (PT) across interfacial (IF) versus in bulk (B) water (10, 14). Because aqueous surfaces are usually charged relative to the bulk liquid (15), the thermodynamic requirement of uniform electrochemical activity throughout (including the interfacial regions) implies that the chemical activity of protons (pH) in IF could be different from that in the B liquid. Reduced hydration of ionic species at the interface could force acids and bases toward their undissociated forms (16).

These fundamental issues have been extensively investigated via electrostatic (17) and electrokinetic experiments (11), surface tension studies and analysis (18, 19), surface-specific spectroscopies (9, 20–22), and theoretical (quantum mechanical and molecular dynamics) calculations (7, 23–25). Some experimental (9) and theoretical (7, 25, 26) results were interpreted to signify that the air–water interface is more acidic than bulk water, whereas others reached the opposite conclusion (8, 11, 21, 23, 27). The impasse stems in part from the failure to recognize that acidity is a relative concept describing the extent of proton sharing between two conjugate acid/base pairs under specified conditions. Theoretical calculations and surface-specific spectroscopies on the structure of interfacial water are therefore moot about its functional acidity. By definition (28), W is a Brønsted base if and only if it can accept protons from Brønsted acids AH, reaction R1

$$AH + W = A^- + WH^+. \qquad \textbf{[R1]}$$

An operational measure of the basicity of W as a medium is given by the acidity constant of AH therein: $K_A = [A^-]\,[WH^+]/[AH]$. If W is bulk water, the acidity constant $K_{A,B}$ can be derived from experimental data on the degree of dissociation: $\theta_B = [A^-]/([A^-]+[AH])$, as a function of pH via Eq. **1**,

$$\theta_B = 1/\left(1 + 10^{pK_A - pH}\right). \qquad \textbf{[1]}$$

A formal extension of Eq. **1** to interfacial water would require (θ_{IF}, pH_{IF}) rather than experimentally accessible (θ_{IF}, pH) data. This is an essential difficulty because the estimation of pH_{IF} from pH_B (16, 29) necessarily involves assumptions about ion distributions and the dielectric properties of water in double layers of molecular dimensions (30–33) (*SI Discussion*). Lacking a thermodynamic pH_{IF} scale based on independent measurements, interfacial acidity constants $K_{A,IF}$ become constructs circularly defined from estimated pH_{IF} values. These simple considerations should make it apparent that conventional concepts on acidity in bulk phases may be meaningless in connection with interfaces.

It is, however, meaningful to ask whether the Brønsted basicity of water is different on either side of water–hydrophobe interfaces. Here we sought to answer this question by performing appropriate experiments. Experiments had to ensure that the acidic probe, AH, would exchange its proton with the interface immediately before the detection of ($A^- + XH^+$) products. Mapping interfacial layers of molecular thicknesses further calls for static molecular probes locked at specified depths, or dynamic ones that interact with the interface during intervals shorter than characteristic diffusion times through the interfacial region. Below, we report experiments in which the production of A^- is monitored as a function of pH via online electrospray ionization mass spectrometry (ESI-MS) of the interfacial layers of injected aqueous jets containing dissolved AH(aq) versus those collided with gaseous AH(g) molecules (Fig. S1 and *SI Methods*) (10, 34). The decisive advantages of online mass spectrometry over spectro-

Author contributions: H.M., S.E., R.J.N., and L.A.S. performed research; H.M., S.E., R.J.N., L.A.S., W.A.G, and A.J.C. analyzed data; M.R.H. contributed new reagents/analytic tools; A.J.C. designed research; and A.J.C. wrote the paper.

The authors declare no conflict of interest.

This article is a PNAS Direct Submission.

[1]To whom correspondence should be addressed. E-mail: ajcoluss@caltech.edu.

This article contains supporting information online at www.pnas.org/lookup/suppl/doi:10.1073/pnas.1209307109/-/DCSupplemental.

scopic techniques are that it (*i*) also operates in situ, but is fast, mass selective, and has high sensitivity, (*ii*) naturally discriminates against a background of neutral AH reactants, and (*iii*) provides unequivocal information about the molecular composition of product ions A^-. We have previously demonstrated the surface specificity of our experiments by showing that (*i*) anion signal intensities in the mass spectra of equimolar salt solutions adhere to a normal Hofmeister series (rather than being identical) (35, 36), and (*ii*) they allow the detection of products of gas–liquid reactions that could only be formed at the air–water interface (37).

Experimental Results

The results of a typical experiment are shown in Fig. 1, in which the formation of hexanoate (A^- in reaction R1, the product of the dissociation of hexanoic acid: $RCOO^-$, $R \equiv C_5H_{11}$, m/z = 115, is detected by online ESI-MS and reported as I_{115} signal intensities) on the surface of aqueous jets (*i*) containing dissolved RCOOH(aq) or (*ii*) externally exposed to RCOOH(g), is plotted as a function of pH. Throughout, pH is the pH of the injected solutions, adjusted with HCl/NaOH and measured with a calibrated pH meter before injection. We found that 50% of the injected RCOOH(aq) dissociates into $RCOO^-$ at $pH_{1/2} = 4.8 \pm 0.2$ (the inflection point of the I_{115} versus pH titration curve), which is identical to the acidity constants, pK_A, of short-chain alkyl carboxylic acids determined by conventional analytical procedures (38). This result corroborates the reliability of our experimental setup and provides a calibration set point for our measurements. The key finding, however, is that RCOOH(g) dissociates upon colliding on the surface of water jets that are ~2 pH units more acidic than in case 1, leading to a titration curve with a $pH_{1/2} = 2.8 \pm 0.2$ midpoint. The second major difference between both experiments is that the limiting I_{115} signals reached above pH ~5 only extend to pH ~9, before increasing again about fivefold above pH ~10 (Fig. 1, *Inset*). This fact indicates that the nature of the W/WH^+ conjugate pair presented by the surface of water to incoming RCOOH(g) changes above pH ~10. To sum up, the results of Fig. 1 represent unambiguous evidence that RCOOH(aq) and RCOOH(g) are deprotonated to significantly different extents on either side of the air–water interface at the same pH. They also confirm that the $RCOO^-$ detected in case 2 are produced on the aerial side of the interface; i.e., before the dissolution of RCOOH(g) in bulk water, because otherwise we should have obtained the same titration curve in both cases. The addition of inert electrolytes, such as NaCl, in the submillimolar range has little effect on these results (Fig. S2). Present results, which are the counterpart of the observations we made in similar experiments involving the protonation of the strong base trimethylamine ($pK_A = 9.8$ in bulk water) on aqueous jets (10), represent an experimental determination of the functional acidity/basicity of the air–water interface.

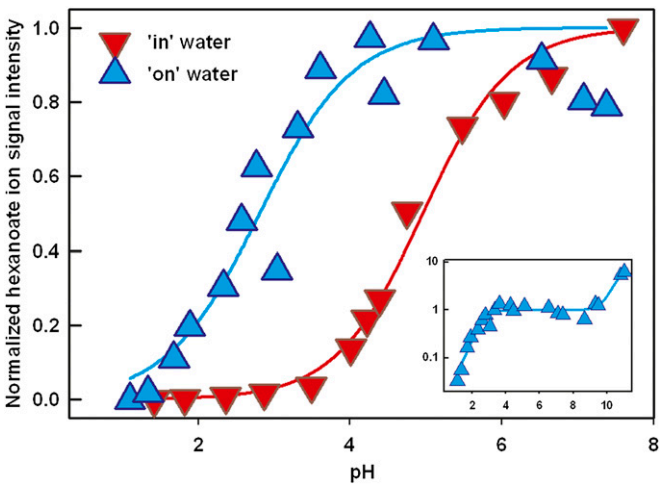

Fig. 1. Normalized electrospray ionization mass-spectral signal intensities of hexanoate ion $RCOO^-$ ($R = C_5H_{11}$, m/z = 115) on the surface of water jets (*i*) containing 1 mM RCOOH(aq) (downward triangles) (*ii*), exposed to 770 ppbv RCOOH(g) (upward triangles) for ~10 μs (1 ppbv = 2.4×10^{10} molecules cm^{-3} at 1 atm, 293 K) as functions of the pH of jet water. Midpoints at (*i*) $pK_A = 4.8 \pm 0.2$, (*ii*) $pH_{1/2} = 2.8 \pm 0.2$. (*Inset*) The results of case (*ii*) experiments carried over a wider pH range.

Fig. 2 shows how $RCOO^-$ increases as a function of the concentration of RCOOH(g) on water jets of three different acidities. It is notable that $RCOO^-$ production plateaus above ~300 ppbv (parts per billion by volume; 1 ppbv = 2.4×10^{10} molecules cm^{-3} at 1 atm, 293 K) RCOOH(g) both at low (pH 2.1) and high (pH 10.1) acidities, but still increases at ~800 ppbv RCOOH(g) over pH 5.1 water. It is apparent that RCOOH(g) does not transfer its proton directly to the aerial side of water; i.e., W in reaction R1 is not H_2O but a more reactive basic species, probably interfacial OH^-, OH^-_{IF}. Furthermore, the production of $RCOO^-$ on the surface of water is limited by the availability of OH^-_{IF} at pH 2.1 and 10.1, and by [RCOOH(g)] (up to and beyond 800 ppbv) at midrange pH values. Regression of the data of Fig. 2 to a Langmuir adsorption functional: $\Gamma = \Gamma_{MAX} \times [RCOOH(g)]/(K_{1/2} + [RCOOH(g)])$, yields: $\Gamma_{MAX} = I_{115,MAX} = 9.1 \times 10^3$, 6.5×10^4, and 7.2×10^4 (in arbitrary units), $K_{1/2}$ = 42, 308, and 46 ppbv at pH 2.1, 5.1, and 10.1, respectively. The physical implications of these results are that (*i*) the surface becomes saturated with OH^-_{IF} at $pH > pH_{1/2} = 2.8$ [because $\Gamma_{MAX}(10.1) \sim \Gamma_{MAX}(5.1) >> \Gamma_{MAX}(2.1)$] and (*ii*) OH^-_{IF} is ~7 times less reactive at pH 5.1 than at pH 10.1 [because $K_{1/2}(5.1)$ is ~7 times larger than $K_{1/2}(10.1)$]. In other words, it is the reactivity of OH^-_{IF} toward RCOOH(g), rather than its concentration, that increases above pH 10.1. The higher reactivity of OH^-_{IF} above pH 10.1 is consistent with its closer approach to an increasingly screened negatively charged interface in more concentrated electrolyte solutions.

The OH^-_{IF} surface density, σ_{OH-IF}, sensed by RCOOH(g) molecules on the aerial side of water could be estimated from the frequency of RCOOH(g) collisions with the surface of the jet given by the kinetic theory of gases: $f[cm^{-2} \cdot s^{-1}] = 1/4\ \gamma\ c\ n$ (*SI Discussion*). We obtain $\sigma_{OH-IF} \sim (3–15) \times 10^9\ OH^-\ cm^{-2}$, at pH 5.1 and 10.1; i.e., a surface-charge density of $\sigma_{qOH} \sim$ (0.5–2.5) $nC \cdot cm^{-2} < 10\ nC \cdot cm^{-2}$. The estimated value of σ_{qOH} is $\sim 10^2$ times smaller than the surface-charge densities $\sigma_\zeta > 1\ \mu C \cdot cm^{-2}$ deduced from the ζ-potentials measured in the electrophoresis of bubbles and oil droplets in water of pH higher than their isoelectric point pI ~3 (8, 11). This discrepancy is deemed significant because it vastly exceeds the combined stated uncertainties of σ_{qOH} and σ_ζ. This issue is analyzed later in the text.

Thermochemical Considerations

The above observations are conveniently framed in terms of the thermodynamics of proton transfer from the prototypical carboxylic acid CH_3COOH to $X = H_2O$ or OH^- (14, 39–41) in the gas-phase reactions R2 and R3

$$CH_3COOH(g) + H_2O(g) = CH_3COO^-(g) + H_3O^+(g) \quad \textbf{[R2]}$$

$$CH_3COOH(g) + OH^-(g) = CH_3COO^-(g) + H_2O(g) \quad \textbf{[R3]}$$

viz.: $\Delta G_2^\circ = 182\ kcal \cdot mol^{-1}$, $\Delta G_3^\circ = -43\ kcal \cdot mol^{-1}$ (39) (1 kcal = 4.18 kJ). The large endoergicity of R2, in which infinitely separated ions are created from neutral species, is reduced by ~100 $kcal \cdot mol^{-1}$ if products are brought to the contact ion–pair

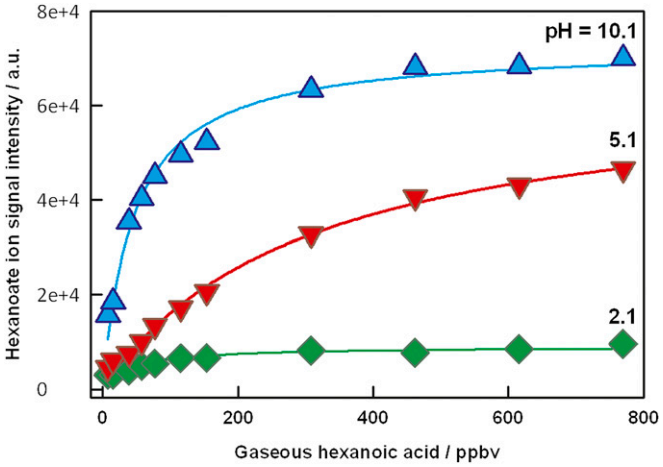

Fig. 2. Electrospray ionization mass-spectral signal intensities of hexanoate ion $RCOO^-$ (R = C_5H_{11}, *m/z* = 115) on the surface of water jets exposed to variable concentrations of RCOOH(g), at pH 2.1, 5.1, and 10.1. Curves correspond to data regressions to Langmuir adsorption isotherms: $\Gamma = \Gamma_{MAX} \times [RCOOH(g)]/\{K_{1/2} + [RCOOH(g)]\}$ $\Gamma_{MAX} = I_{115,MAX} = 9.1 \times 10^3$, 6.5×10^4, and 7.2×10^4 (in arbitrary units); $K_{1/2}$ = 42, 308, and 46 ppbv at pH 2.1, 5.1, and 10.1, respectively.

separations (~3 Å) reached in the early stages of proton transfer (41). The participation of six additional H_2O molecules leading to partially hydrated clusters consisting of $[CH_3COO^-{\cdot}(H_2O)_3 + H_3O^+{\cdot}(H_2O)_3]$ contact ion pairs is sufficient to render R2 exoergic (40). Of course, exoergic proton transfer could nevertheless be hindered by a significant kinetic barrier that would prevent R2 from proceeding fast enough during $CH_3COOH(g)$ collisions with the surface of water (42, 43). Reaction R3, in contrast, is exoergic as written, spontaneous both in gas phase and in aqueous solution, and therefore expected to proceed readily at the interface. To provide a molecular underpinning to these arguments we carried out quantum-mechanical calculations on model water clusters.

Quantum-Mechanical Calculations

We carried out density functional theory quantum-mechanical calculations at the M06/6–311G**++ level. M06 is a hybrid metageneralized gradient approximation (meta-GGA) functional including both a kinetic-energy density functional and exact Hartree–Fock exchange energy. Various groups, including ours, have confirmed that M06 provides the best description of hydrogen bonding, internuclear distances, and chemical kinetics in water clusters compared with other GGA, (empirically) dispersion corrected GGA, meta, or hybrid-GGA functional (44, 45). Here we considered 20-molecule neat-water clusters W20 (W = H_2O), and clusters containing an additional OH^- ion, $W_{20}{\cdot}OH^-$. For the $W_{20}{\cdot}OH^-$ cluster we find that the excess OH^- ion prefers to be at the surface of the cluster. Thus, our model system provides the OH^- at the air–water interface required to explain the interfacial chemistry observed in our experiments. Furthermore, we have recently shown that small water clusters treated at the B3LYP/6–311G**++ level of theory provide a satisfactory description of interfacial proton transfer at air–water interface (46).

For pure water, we found that (*i*) CH_3COOH coordinates to the surface of W_{20} producing weakly bound adducts $[CH_3COOH{\cdots}W_{20}]$; and (*ii*) for a variety of $[CH_3COO^-{\cdots}W_{19}{\cdot}H_3O^+]$ initial structures in which CH_3COO^- is placed on the periphery of $W_{19}{\cdot}H_3O^+$ we find that all relax spontaneously to $[CH_3COOH{\cdots}W_{20}]$. These results indicate the existence of a significant barrier for CH_3COOH dissociation on the surface of pure water, which is not lowered by the presence of strong acid anions such as Cl^- [$pK_A(HCl) = -7 << 4.8$] (Fig. S3). This contrasts with our observations on the dissociation of the strong HNO_3 at the air–water interface (14). This dissociation of the weak CH_3COOH on the surface of water is hindered by the intrinsic kinetic barrier limiting this process "in water" [a process previously investigated via Car–Parrinello quantum-mechanical metadynamics (43)], and by the additional cost of creating a cavity to accommodate the resulting CH_3COO^- inside the bulk liquid (14). In the case of a $W_{20}{\cdot}OH^-$ water cluster, the reaction coordinate for proton transfer from CH_3COOH to $W_{20}{\cdot}OH^-$ involves three or four water molecules, leading to a negligible kinetic barrier and stable reaction products on both free-energy and enthalpy surfaces (Fig. 3). We find that these results depend little on the various close-lying energy minima or the anharmonicity of low-frequency vibrations in $W_n{\cdot}OH^-$ clusters (47). Because $\Delta G_3^\circ = -43$ kcal mol^{-1}, it is quite plausible that an OH^- located near the interface would induce barrierless PT.

The mechanism by which anions (including OH^-) are driven to the interfacial region, however, falls outside the scope of this study (23, 35, 36, 48), which is to investigate the pH dependence of RCOOH dissociation on both sides of the air–water interface. The type and hierarchy of the interactions (electrostatic, inductive, hydrogen bonding, and dispersive interactions) responsible for driving OH^- to the interface are not fully resolved by current density functionals (7, 44, 49–52).

Discussion

our reactive gas–liquid experiments demonstrate that OH^-_{IF} ions become available to RCOOH (pK_A = 4.8 in bulk water) on the aerial side of pH > 2 water. Similar experiments in our laboratory involving the protonation of gaseous trimethylamine (pK_A = 9.8 in bulk water) have shown that $H_3O^+_{IF}$ ions become available on the surface of pH < 4 water (10). We conclude that the pH at which $[H_3O^+_{IF}]$ and $[OH^-_{IF}]$ balance each other on the aerial side of water, the point of zero charge, is pH_{PZC} ~3. It is significant that this value coincides with the isoelectric point of water, pI ~3, measured at the shear plane of air bubbles (53) and of hydrophobic oil drops (11) in electrophoretic experiments (54). The "shear plane" is the outer surface of the water shells that move along with bubbles and drops migrating in an externally applied electric field; it lies a few nanometers (nm) away from the interface proper (8, 11). Because RCOOH(g) is a specific probe for OH^-_{IF} [recall that PT from RCOOH(g) to the surface of water is kinetically hindered regardless of the orientation of water molecules therein], whereas electrophoretic measurements report net electric charge, the essential coincidence of pH_{PZC} and pI values suggests that the negative charge of the air–water interface above pH ~2.5 may be ascribed to the presence of excess interfacial OH^-_{IF} (8, 11). This view is consistent with the fact that negative ζ-potentials of colloidal drops and bubbles in the static electric fields of electrophoretic experiments require the presence of negatively charged discrete entities that can migrate independently of their counterions, such as OH^-, rather than of inward-pointing water dipoles or charge-transfer $[H_2O^-{\cdots}H_2O^+]$ moieties (55–58). A potential role for hydrated electrons, $H_2O{\cdot}e^-$, as discrete carriers can be discarded because their formation via $3\ H_2O = H_2O{\cdot}e^- + H_3O^+ + {\cdot}OH$, is thermodynamically forbidden under ambient conditions (56, 59, 60).

Some surface-specific nonlinear spectroscopic studies (9, 61), most theoretical calculations (7, 51, 62), and the ion partitioning analysis of surface tension data on electrolyte solutions (19) have predicted the accumulation of H_3O^+ at and the exclusion of OH^- from the air–water interface. On the basis of such evidence it has been argued that water surface is acidic (7, 25). It should be apparent by now that "acid" and "basic" qualifiers designate the ability of certain bodies, the air–water interface in this case,

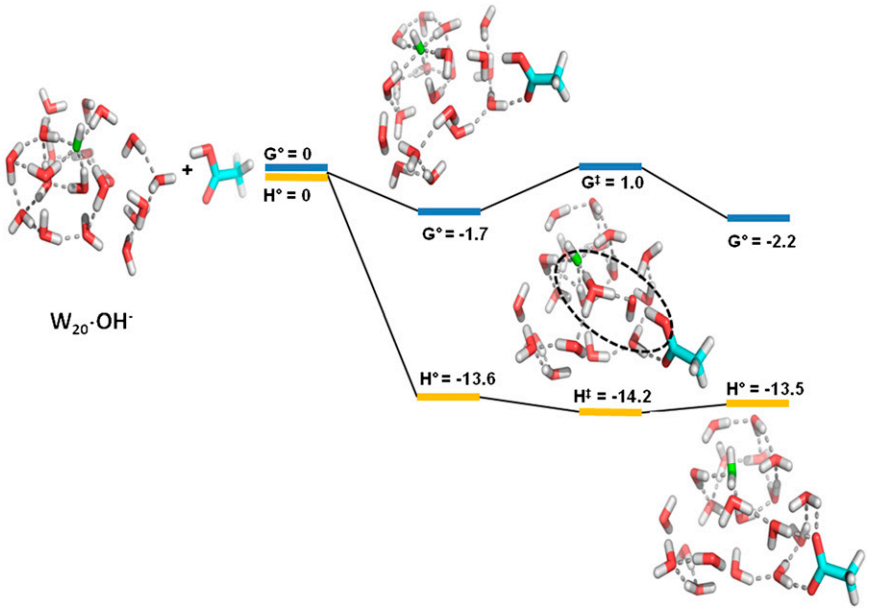

Fig. 3. Calculated Gibbs free energies (G°) and enthalpies (H°) (in kcal·mol^{-1}) of reactants, adducts, transition states, and products of optimized water clusters containing hydroxide, $W_{20}{\cdot}OH^-$ in contact with acetic acid. Calculations in the absence of OH^- did not yield stable [$CH_3COO^- + H_3O^+$] dissociation products.

to exchange protons with other entities under specific conditions and, therefore, strictly apply to chemical reactions rather than to structural features.

The finding that the charge density on the aerial side of the interface, σ_{qOH}, estimated from our reactive gas–liquid experiments is considerably smaller than that detected at the shear hydrodynamic plane, σ_ζ, suggests the existence of nonmonotonic OH^-_{IF} vertical profiles. We have recently shown that different anions populate interfacial layers at depths that are inversely correlated with their relative surface affinities (63). The emerging picture is that surface affinities indicate how close anions approach the interface rather than their relative concentrations within a single subsurfacial layer. Thus, the possibility arises that ion concentration profiles within interfacial double layers could be nonmonotonic (31) and, as a result, experiments probing water basicity at different depths could lead to dissimilar results. One corollary is that the low affinity of OH^- for the air–water interface predicated by some calculations (7, 25) and implied by some surface-specific spectroscopies (9) is not in principle incompatible with the sizable charge densities deduced from electrophoretic experiments (8). Note that these arguments are conditional, because the reported electrophoretic σ_ζ values are derived from experimental ζ-potentials by using a continuous Gouy–Chapman model for the double layer based on the dielectric constant of bulk water (31, 32) and are, as such, susceptible to major revision.

Because our experimental results are based on sampling the composition of the surface of nascent water jets exposed to RCOOH(g) within a few tens of microseconds after emerging from the nozzle, whereas electrophoretic experiments involve much longer time scales, the finding that $pH_{PZC} \sim pI$ seems to suggest that equilibrium is established in both cases. Note however that the OH^- ions populating the air–water interfaces monitored in our experiments must then be produced at faster rates than those estimated from the dissociation of bulk water: $2\ H_2O = H_3O^+ + OH^-$, whose characteristic e times: $\tau_{dissociation} = k_{forward}^{-1} = (K_w\ k_{backward})^{-1} \sim (10^{-14} \times 10^{11}\ M^{-1}{\cdot}s^{-1})^{-1} = 10^3$ s (64, 65), vastly exceed the lifetimes of our water jets (7). Water autolysis concurrent with OH^- diffusion and binding at the interface may effectively shorten relaxation times into the submillisecond timescale (54), but other explanations are possible (66). This important issue is being investigated in our laboratory.

To sum up, we (*i*) demonstrate the presence of hydroxide ions on the aerial surface of pH > 2 water, (*ii*) ascribe the negative charge of the surface of neat water to excess OH^-, (*iii*) infer the existence of nonmonotonic OH^- profiles through interfacial water layers, and (*iv*) determine a point of zero charge $pH_{PZC} \sim 3$ for water–hydrophobe interfaces that is consistent with the value obtained in the electrophoresis of bubbles and oil droplets.

Methods

Experimental Procedures. Gas–liquid experiments were conducted by intersecting free-flowing aqueous jets with $C_5H_{11}COOH(g)/N_2(g)$ beams in a chamber held at 1 atm, 293 K, and detecting the formation of $C_5H_{11}COO^-$ therein via online ESI-MS. Our ESI mass spectrometer, which has been described in detail elsewhere (10, 14, 34), is configured to report the ion composition of the net charges generated from the fragmentation of the primary drops sheared from the jet by a fast coaxial annular nebulizer gas flow (67, 68). This claim has been previously validated by showing that (*i*) the relative anion abundances at air–water interface, i.e., the mass-spectral signal intensities, measured on aqueous jets consisting of equimolar solutions of mixed salts follow a normal Hofmeister series (as expected at the air–water interface and confirmed by other surface-sensitive techniques) and are specifically affected by cationic or anionic surfactants (36), (*ii*) mass spectra of aqueous jets exposed to reactive gases detect species necessarily produced at the gas–liquid interface rather than in bulk water. For further details see *SI Methods*.

Computational Details. Gibbs free energies (G) at 298 K were computed from calculated enthalpies (H) and entropies (S) according to $G = E_{elec} + ZPE + H_{vib} - TS_{vib}$. Geometries of energy minima states were optimized using the M06 functional (44) and 6–311G** basis (69) for all atoms. After geometry optimization, the electronic energy E_{elec} was evaluated with the 6–311G**++ basis (70) The Hessians at these geometries were used to determine that the minima and transition states led to 0 and 1 imaginary frequency, respectively. Vibrational frequencies provided zero-point energies and vibrational contributions to enthalpies and entropies. The free energies of acetic acid at 1 atm were calculated using statistical mechanics for ideal gases.

ACKNOWLEDGMENTS. Our research is supported by Japan Society for the Promotion of Sciences Postdoctoral Fellowship for Research Abroad (to S.E.) and National Science Foundation Grant AGS—964842a (to M.R.H.).

1. Warshel A, et al. (2006) Electrostatic basis for enzyme catalysis. *Chem Rev* 106(8): 3210–3235.
2. Mulkidjanian AY, Heberle J, Cherepanov DA (2006) Protons @ interfaces: Implications for biological energy conversion. *Biochim Biophys Acta Bioenerg* 1757:913–930.
3. Sandén T, Salomonsson L, Brzezinski P, Widengren J (2010) Surface-coupled proton exchange of a membrane-bound proton acceptor. *Proc Natl Acad Sci USA* 107(9): 4129–4134.
4. Bell RC, Wu K, Iedema MJ, Schenter GK, Cowin JP (2009) The oil-water interface: Mapping the solvation potential. *J Am Chem Soc* 131(3):1037–1042.
5. Ariga K, Nakanishi T, Hill JP (2006) A paradigm shift in the field of molecular recognition at the air-water interface: From static to dynamic. *Soft Matter* 2(6):465–477.
6. McGorty R, Fung J, Kaz D, Manoharan VN (2010) Colloidal self-assembly at an interface. *Mater Today* 13:34–42.
7. Buch V, Milet A, Vácha R, Jungwirth P, Devlin JP (2007) Water surface is acidic. *Proc Natl Acad Sci USA* 104(18):7342–7347.
8. Beattie JK, Djerdjev AM, Warr GG (2009) The surface of neat water is basic. *Faraday Discuss* 141:31–39, and discussion 81–98.
9. Petersen PB, Saykally RJ (2008) Is the liquid water surface basic or acidic? Macroscopic vs. molecular-scale investigations. *Chem Phys Lett* 458:255–261.
10. Enami S, Hoffmann MR, Colussi AJ (2010) Proton availability at the air/water interface. *J Phys Chem Lett* 1:1599–1604.
11. Marinova KG, et al. (1996) Charging of oil-water interfaces due to spontaneous adsorption of hydroxyl ions. *Langmuir* 12:2045–2051.
12. Stiopkin IV, et al. (2011) Hydrogen bonding at the water surface revealed by isotopic dilution spectroscopy. *Nature* 474(7350):192–195.
13. Mulkidjanian AY (2006) Proton in the well and through the desolvation barrier. *Biochim Biophys Acta* 1757(5-6):415–427.
14. Mishra H, et al. (2012) Anions dramatically enhance proton transfer through aqueous interfaces. *Proc Natl Acad Sci USA* 109(26):10228–10232.
15. Fawcett WR (2008) The ionic work function and its role in estimating absolute electrode potentials. *Langmuir* 24(17):9868–9875.
16. Zhao XL, Subrahmanyan S, Eisenthal KB (1990) Determination of pK_a at the air/water interface by second harmonic generation. *Chem Phys Lett* 171:558–562.
17. Jarvis NL, Scheiman MA (1968) Surface potentials of aqueous electrolyte solutions. *J Phys Chem* 72:74–80.
18. Petersen PB, Saykally RJ (2005) Adsorption of ions to the surface of dilute electrolyte solutions: The Jones-Ray effect revisited. *J Am Chem Soc* 127(44):15446–15452.
19. Pegram LM, Record MT (2008) Quantifying accumulation or exclusion of H^+, HO^-, and Hofmeister salt ions near interfaces. *Chem Phys Lett* 467:1–8.
20. Tian CS, Ji N, Waychunas GA, Shen YR (2008) Interfacial structures of acidic and basic aqueous solutions. *J Am Chem Soc* 130(39):13033–13039.
21. Tian CS, Shen YR (2009) Structure and charging of hydrophobic material/water interfaces studied by phase-sensitive sum-frequency vibrational spectroscopy. *Proc Natl Acad Sci USA* 106(36):15148–15153.
22. Byrnes SJ, Geissler PL, Shen YR (2011) Ambiguities in surface nonlinear spectroscopy calculations. *Chem Phys Lett* 516:115–124.
23. Gray-Weale A, Beattie JK (2009) An explanation for the charge on water's surface. *Phys Chem Chem Phys* 11(46):10994–11005.
24. Kudin KN, Car R (2008) Why are water-hydrophobic interfaces charged? *J Am Chem Soc* 130(12):3915–3919.
25. Iuchi S, Chen HN, Paesani F, Voth GA (2009) Hydrated excess proton at water-hydrophobic interfaces. *J Phys Chem B* 113(13):4017–4030.
26. Vácha R, Buch V, Milet A, Devlin JP, Jungwirth P (2007) Autoionization at the surface of neat water: Is the top layer pH neutral, basic, or acidic? *Phys Chem Chem Phys* 9(34):4736–4747.
27. Zangi R, Engberts JBFN (2005) Physisorption of hydroxide ions from aqueous solution to a hydrophobic surface. *J Am Chem Soc* 127(7):2272–2276.
28. Nic M, Jirat J, Kosata B, Jenkins A (2006) *IUPAC Compendium of Chemical Terminology* (Blackwell Scientific, Oxford).
29. Zhao XL, Ong SW, Wang HF, Eisenthal KB (1993) New method for determination of surface pK_A using 2^{nd} harmonic generation. *Chem Phys Lett* 214:203–207.
30. Rowlinson JS, et al. (1981) Structure of the interfacial region—General discussion. *Faraday Symp Chem Soc S* 16:205–256.
31. Luo GM, et al. (2006) Ion distributions near a liquid-liquid interface. *Science* 311 (5758):216–218.
32. Netz RR, Orland H (2000) Beyond Poisson-Boltzmann: Fluctuation effects and correlation functions. *Eur Phys J E* 1:203–214.
33. Cherepanov DA (2004) Force oscillations and dielectric overscreening of interfacial water. *Phys Rev Lett* 93(26):266104-1–266104-4.
34. Enami S, Stewart LA, Hoffmann MR, Colussi AJ (2010) Superacid chemistry on mildly acidic water. *J Phys Chem Lett* 1:3488–3493.
35. Cheng J, Hoffmann MR, Colussi AJ (2008) Anion fractionation and reactivity at air/water: Methanol interfaces. Implications for the origin of Hofmeister effects. *J Phys Chem B* 112(24):7157–7161.
36. Cheng J, Vecitis CD, Hoffmann MR, Colussi AJ (2006) Experimental anion affinities for the air/water interface. *J Phys Chem B* 110(51):25598–25602.
37. Enami S, Hoffmann MR, Colussi AJ (2008) Acidity enhances the formation of a persistent ozonide at aqueous ascorbate/ozone gas interfaces. *Proc Natl Acad Sci USA* 105(21):7365–7369.
38. Haynes WM (2012) *Handbook of Chemistry and Physics* (Taylor and Francis, London).
39. Hunter EPL, Lias SG (1998) Evaluated gas phase basicities and proton affinities of molecules: An update. *J Phys Chem Ref Data* 27:413–656.
40. Meot-Ner M (2005) The ionic hydrogen bond. *Chem Rev* 105(1):213–284.
41. Leopold KR (2011) Hydrated acid clusters. *Annu Rev Phys Chem* 62:327–349.
42. Nguyen S, Fenn JB (2007) Gas-phase ions of solute species from charged droplets of solutions. *Proc Natl Acad Sci USA* 104(4):1111–1117.
43. Park JM, Laio A, Iannuzzi M, Parrinello M (2006) Dissociation mechanism of acetic acid in water. *J Am Chem Soc* 128(35):11318–11319.
44. Zhao Y, Truhlar DG (2008) The M06 suite of density functionals for main group thermochemistry, thermochemical kinetics, noncovalent interactions, excited states, and transition elements: Two new functionals and systematic testing of four M06-class functionals and 12 other functionals. *Theor Chem Acc* 120:215–241.
45. Bryantsev VS, Diallo MS, van Duin ACT, Goddard WA (2009) Evaluation of B3LYP, X3LYP, and M06-class density functionals for predicting the binding energies of neutral, protonated, and deprotonated water clusters. *J Chem Theory Comput* 5: 1016–1026.
46. Mishra H, Nielsen RJ, Enami S, Hoffmann MR, Goddard WA III, Colussi AJ (2012) Quantum chemical insights into the dissociation of nitric acid on the surface of aqueous electrolytes. *Int J Theor Chem*, 10.1002/qua.24151.
47. Maheshwary S, Patel N, Sathyamurthy N, Kulkarni AD, Gadre SR (2001) Structure and stability of water clusters $(H_2O)_n$, n = 8-20: An ab initio investigation. *J Phys Chem A2* 105:10525–10537.
48. Otten DE, Shaffer PR, Geissler PL, Saykally RJ (2012) Elucidating the mechanism of selective ion adsorption to the liquid water surface. *Proc Natl Acad Sci USA* 109(3): 701–705.
49. Grimme S (2006) Semiempirical GGA-type density functional constructed with a long-range dispersion correction. *J Comput Chem* 27(15):1787–1799.
50. Dahlke EE, Truhlar DG (2005) Improved density functionals for water. *J Phys Chem B* 109(33):15677–15683.
51. Mundy CJ, Kuo IFW, Tuckerman ME, Lee HS, Tobias DJ (2009) Hydroxide anion at the air-water interface. *Chem Phys Lett* 481:2–8.
52. Jungwirth P, Tobias DJ (2006) Specific ion effects at the air/water interface. *Chem Rev* 106(4):1259–1281.
53. Takahashi M (2005) ζ potential of microbubbles in aqueous solutions: Electrical properties of the gas-water interface. *J Phys Chem B* 109(46):21858–21864.
54. Liu M, Beattie JK, Gray-Weale AA (2012) The surface relaxation of water. *J Phys Chem B* 116(30):8981–8988.
55. Vácha R, et al. (2011) The orientation and charge of water at the hydrophobic oil droplet-water interface. *J Am Chem Soc* 133(26):10204–10210.
56. Ben-Amotz D (2011) Unveiling electron promiscuity. *J Phys Chem Lett* 2:1216–1222.
57. Kuhne TD, Pascal TA, Kaxiras E, Jung Y (2011) New insights into the structure of the vapor/water interface from large-scale first-principles simulations. *J Phys Chem Lett* 2: 105–113.
58. Vácha R, et al. (2012) Charge transfer between water molecules as the possible origin of the observed charging at the surface of pure water. *J Phys Chem Lett* 3:107–111.
59. Zhan CG, Dixon DA (2003) The nature and absolute hydration free energy of the solvated electron in water. *J Phys Chem B* 107:4403–4417.
60. Buchner F, Schultz T, Lübcke A (2012) Solvated electrons at the water-air interface: Surface versus bulk signal in low kinetic energy photoelectron spectroscopy. *Phys Chem Chem Phys* 14(16):5837–5842.
61. Petersen PB, Saykally RJ (2006) Probing the interfacial structure of aqueous electrolytes with femtosecond second harmonic generation spectroscopy. *J Phys Chem B* 110 (29):14060–14073.
62. Takahashi H, et al. (2011) Energetic origin of proton affinity to the air/water interface. *J Phys Chem B* 115(16):4745–4751.
63. Enami S, Mishra H, Hoffmann MR, Colussi AJ (2012) Hofmeister effects in micromolar electrolyte solutions. *J Chem Phys* 136(15):154707-1–154707-5.
64. Geissler PL, Dellago C, Chandler D, Hutter J, Parrinello M (2001) Autoionization in liquid water. *Science* 291(5511):2121–2124.
65. Hassanali A, Prakash MK, Eshet H, Parrinello M (2011) On the recombination of hydronium and hydroxide ions in water. *Proc Natl Acad Sci USA* 108(51):20410–20415.
66. Donten ML, Vandevondele J, Hamm P (2012) Speed limits for acid-base chemistry in aqueous solutions. *Chimia (Aarau)* 66(4):182–186.
67. Theofanous TG, et al. (2012) The physics of aerobreakup. II. Viscous liquids. *Phys Fluids* 24:022104-1–022104-39.
68. Zilch LW, Maze JT, Smith JW, Ewing GE, Jarrold MF (2008) Charge separation in the aerodynamic breakup of micrometer-sized water droplets. *J Phys Chem A* 112(51): 13352–13363.
69. Francl MM, et al. (1982) Self-consistent molecular-orbital methods. 23. A polarization-type basis set for 2^{nd} row elements. *J Chem Phys* 77:3654–3665.
70. Clark T, Chandrasekhar J, Spitznagel GW, Schleyer PV (1983) Efficient diffuse function-augmented basis sets for anion calculations. 3. The 3-21+G basis set for 1^{st} row elements, Li-F. *J Comput Chem* 4:294–301.

Supporting Information

Mishra et al. 10.1073/pnas.1209307109

SI Methods

Experimental Procedures. An electrospray ionization mass spectrometer (Hewlett-Packard-1100 MSD) consisting of an atmospheric pressure spraying chamber of orthogonal ion-sampling geometry was used in this study (1). The orthogonal orientation of the liquid jet relative to the inlet to the mass spectrometer ensures that only a small fraction of analyte, sheared from the jet periphery by a nebulizer gas, is analyzed. Gas–liquid interfacial reactions were investigated in experiments in which pH-adjusted aqueous jets were intersected with beams of carboxylic acid (RCOOH) vapors. A schematic diagram of our experimental setup is shown in Fig. S1. The pH-adjusted aqueous solutions were pumped (at 50 $\mu L \cdot min^{-1}$ using a Harvard Apparatus syringe pump) into the electrospray chamber through an electrically grounded stainless steel capillary injector (150 μm external diameter, 100 μm bore). This capillary was surrounded by a coaxial sheath (250 μm internal diameter) issuing N_2 nebulizer gas at 0.5 $L \cdot min^{-1}$. RCOOH vapor beams were produced by sparging N_2 gas through liquid acids or their aqueous solutions maintained at constant temperature. This arrangement guarantees that RCOOH molecules hit the surface of the microjet before being incorporated into the bulk liquid. A fraction of gas–liquid collisions results in proton transfers from RCOOH to the surface of the jet, followed by online mass-spectrometric detection of the $RCOO^-$ produced therein. Because mass spectrometers only detect charged species, our technique requires the separation of anions from cations present in the electroneutral aqueous jet. Charge separation is achieved during jet nebulization in which part of the kinetic energy of the high-speed nebulizer gas is converted into surface and electrostatic energy of the droplets sheared off the outermost layers of the aqueous jets (2–4). As a result, some of the resulting droplets have excess positive or negative charges (5) proportional to ion concentrations in the interfacial layers. We have confirmed the surface sensitivity of our experiments by showing that (*i*) sampled anions are fractionated following a normal Hofmeister series during the nebulization of equimolar salt solutions (6–10), (*ii*) mass spectra are specifically affected by added cationic or anionic surfactants (11–13), (*iii*) we are able to detect the products of gas–liquid reactive collisions, including the protonation of gas–phase bases (12), weak carboxylic acids (12), isoprene (14), and the dissociation of the strong nitric acid at air–water interface (15). Typical experimental conditions are as follows: drying gas rate: 10 $L \cdot min^{-1}$, drying gas temperature: 340 °C, inlet voltage: −3.5 kV relative to ground, fragmentor voltage: 26 V. Hexanoic acid (99%; Sigma-Aldrich) and acetic acid (99%; Sigma-Aldrich) were used as received. All solutions were prepared in deionized water (resistivity 18.2 MΩ cm) from a Millipore Milli-Q gradient system. Solution pH was adjusted by adding concentrated HCl or NaOH solutions and measured with a calibrated pH meter (VWR). Fig. 1 shows a schematic of how charge separation is accomplished via pneumatic shearing of a slow-moving (~0.1 $m \cdot s^{-1}$) analyte jet by the fast annular nebulizer gas (~250 $m \cdot s^{-1}$).

As the smaller charged drops progress toward mass-spectrometer inlet, rapid solvent evaporation is promoted by the drying gas. Within ~100 μs, drops' radii shrink to the Rayleigh limit, given by $q = 8\pi(\varepsilon\ \gamma\ R^3)^{1/2}$ at which the Coulombic repulsions between excess charges in the drop overwhelm surface tension, whereby the charged drops fission into smaller charged drops (2). Here q is the charge on the droplet, ε is the dielectric permittivity, γ is the surface tension of the solvent, and R is the drop radius. Notice that these electrostatic (Coulomb) explosions do not separate negative from positive charges, but only the excess charges of the same sign acquired during the jet breakup by the nebulizer. Also notice that anions may recombine with remaining counterions (or associate with neutrals) in shrinking charged droplets, but the net ions drawn per unit time from the initial jet, $j[(RCOOH)_a(H_2O)_b\ RCOO^-]$ [ions × $time^{-1}$], is conserved in sprays of noninteracting droplets. As the smaller droplets undergo further evaporation, eventually the excess ions are ejected into the gas phase and become amenable for mass-spectrometric detection. The electrokinetic phenomena observed by Saykally and coworkers in a similar setup (16) occur at liquid jet speeds ~500 times higher than in our experiments.

Computational Details. Energy-optimized water clusters with 10 and 20 molecules, W_{10} and W_{20} respectively, were used to gain insight into the proton transfer process at molecular level. In the chosen configurations each water-molecule hydrogen bonds with three neighboring water molecules. Insertion of an OH^- into W_{10} and W_{20}, representative of air–water interfaces of bulk systems with high and low basicity, respectively, leads to a relaxed $(OH \cdot W_n)^-$ structures with OH^- emerging to the surface of the cluster and hydrogen bonded to five water molecules. Anions exhibiting propensity for air–water interface have been reported by experiments and theoretical calculations (17–19). Incipient RCOOH(g) molecule binds to the pure water cluster into optimized adducts (W_n.RCOOH) via two hydrogen bonds with the release of $\Delta H^0 = -8.3$ kcal/mol and $\Delta G^0 = 2.9$ kcal/mol (due to loss in translational entropy). The counterion to OH^- in our experiments, Na^+, was not included in the calculations with small water clusters because they are expected to be separated by distances much larger than our small-sized model. Due to electrostatic bias, water molecules surrounding OH^- become better proton acceptors. We recently reported that proton transfer from gas-phase molecules of a strong acid, HNO_3(g), alighting aqueous surfaces could be catalyzed by interfacial anions, Cl^-. In absence of interfacial Cl^-, the proton transfer to the surface of water was minimal due to a large kinetic barrier. In case of weak acids, RCOOH(g), we observe that

i) Proton transfers from interfacial RCOOH to pure water is hindered by a large kinetic barrier. All calculations with pure water clusters (W10 and W20) optimizing geometries with $RCOO^-$ and H3O+ separated by one to four layers of water molecules relaxed back to undissociated RCOOH and Wn.

ii) Unlike the case of HNO_3(g) on aqueous surface, wherein proton transfer to water was catalyzed by interfacial Cl^-, in case of RCOOH(g) there are kinetic and thermodynamic barriers for analogous proton transfer with interfacial Cl^- (Fig. S3). In other words, the electrostatic bias and concomitant solvent rearrangements by interfacial Cl^- are inadequate to catalyze proton transfer from a weak acid.

iii) $W_{10} \cdot OH^-$ clusters were chosen to represent the surface of water with bulk pH ~12. On this cluster, the dissociation of interfacial RCOOH was spontaneous (Fig. 3*B*).

iv) $W_{20} \cdot OH^-$clusters were chosen to represent the surface of mildly acidic water (pH ~4). We found stable dissociation products with proton transferred to OH^- and $RCOO^-$ located outside water cluster (Fig. 3*A*). Reactants and products were separated by a transition state, searched by optimizing structures in which the two O–H bonds connecting RCOOH with hydronium were constrained, until the chosen set of constraints led to an imaginary frequency vibration. The path

of steepest ascent is then followed by tracking the eigenvector of the motion associated with the imaginary frequency, until an energy maximum is found. Full Hessian harmonic calculations were then performed for the transition state (TS) structures.

SI Discussion

The OH^-_{IF} surface density, σ_{OH-IF}, sensed by RCOOH(g) molecules on the aerial side of water could be estimated from the frequency of RCOOH(g) collisions with the surface of the jet given by the kinetic theory of gases: $f[cm^{-2}{\cdot}s^{-1}] = 1/4\ \gamma\ c\ n$. Here $\gamma \sim 0.05$ is the reactive uptake coefficient of RCOOH(g) on $4 < pH < 8$ water [i.e., we adopt the value measured by Hu et al., for CH_3COOH(g) on neutral water at 293 K] (20), $c = 2.4 \times 10^4$ $cm{\cdot}s^{-1}$ is the mean thermal molecular speed of RCOOH(g) at 300 K, and n its number density in molecules cm^{-3} (21). For estimated gas–liquid contact times of $\tau \sim$10–50 μs (14, 22), at $n \sim K_{1/2} = 1.0 \times 10^{12}$ molecules cm^{-3} (at pH 5.1 and 10.1) we obtain: $\sigma_{OH-IF} = f \times \tau \sim (3–15) \times 10^9$ OH^- cm^{-2}, or a surface-charge density of $\sigma_{qOH} \sim (0.5–2.5)$ $nC{\cdot}cm^{-2} < 10$ nanoCoulomb $(nC){\cdot}cm^{-2}$.

The evaluation of pH_{IF} from pH_B measurements requires assumptions about (*i*) the charge distribution and dielectric properties of water in the interfacial double layer, (*ii*) whether they should be treated as continuous and monotonic functions of depth, and (*iii*) whether surface polarization is due to the unmatched distributions of the intrinsic H^+/OH^- ions at the interface and/or the preferential orientation of water dipoles therein (23–26). All of the above issues remain outstanding at present (23–29).

1. Manisali I, Chen DDY, Schneider BB (2006) Electrospray ionization source geometry for mass spectrometry: Past, present and future. *Trends Anal Chem* 25: 243–256.
2. Kebarle P, Peschke M (2000) On the mechanisms by which the charged droplets produced by electrospray lead to gas phase ions. *Anal Chim Acta* 406:11–22.
3. Kebarle P, Tang L (1993) From ions in solution to ions in the gas-phase—The mechanism of electrospray mass-spectrometry. *Anal Chem* 65:A972.
4. Nguyen S, Fenn JB (2007) Gas-phase ions of solute species from charged droplets of solutions. *Proc Natl Acad Sci USA* 104(4):1111–1117.
5. Zilch LW, Maze JT, Smith JW, Ewing GE, Jarrold MF (2008) Charge separation in the aerodynamic breakup of micrometer-sized water droplets. *J Phys Chem A* 112(51): 13352–13363.
6. Hofmeister F (1888) Zur Lehre von der Wirkung der Salze [The theory of the action of the salts]. *Arch Exp Pathol Pharmakol (Leipzig)* 24:247, German.
7. Otten DE, Shaffer PR, Geissler PL, Saykally RJ (2012) Elucidating the mechanism of selective ion adsorption to the liquid water surface. *Proc Natl Acad Sci USA* 109(3): 701–705.
8. Petersen PB, Saykally RJ (2004) Confirmation of enhanced anion concentration at the liquid water surface. *Chem Phys Lett* 397:51–56.
9. Petersen PB, Saykally RJ (2005) Adsorption of ions to the surface of dilute electrolyte solutions: The Jones-Ray effect revisited. *J Am Chem Soc* 127(44):15446–15452.
10. Tian CS, Byrnes SJ, Han HL, Shen YR (2011) Surface propensities of atmospherically relevant ions in salt solutions revealed by phase-sensitive sum frequency vibrational spectroscopy. *J Phys Chem Lett* 2:1946–1949.
11. Enami S, Vecitis CD, Cheng J, Hoffmann MR, Colussi AJ (2008) Mass spectrometry of interfacial layers during fast aqueous aerosol/ozone gas reactions of atmospheric interest. *Chem Phys Lett* 455:316–320.
12. Enami S, Hoffmann MR, Colussi AJ (2008) Ozonolysis of uric acid at the air/water interface. *J Phys Chem B* 112(14):4153–4156.
13. Kinugawa T, et al. (2011) Conversion of gaseous nitrogen dioxide to nitrate and nitrite on aqueous surfactants. *Phys Chem Chem Phys* 13(11):5144–5149.
14. Enami S, Mishra H, Hoffmann MR, Colussi AJ (2012) Protonation and oligomerization of gaseous isoprene on mildly acidic surfaces: Implications for atmospheric chemistry. *J Phys Chem A* 116(24):6027–6032.
15. Mishra H, et al. (2012) Anions dramatically enhance proton transfer through aqueous interfaces. *Proc Natl Acad Sci USA* 109(26):10228–10232.
16. Duffin AM, Saykally RJ (2007) Electrokinetic hydrogen generation from liquid water microjets. *J Phys Chem C* 111:12031–12037.
17. Cheng J, Hoffmann MR, Colussi AJ (2008) Anion fractionation and reactivity at air/water: Methanol interfaces. Implications for the origin of Hofmeister effects. *J Phys Chem B* 112(24):7157–7161.
18. Cheng J, Vecitis CD, Hoffmann MR, Colussi AJ (2006) Experimental anion affinities for the air/water interface. *J Phys Chem B* 110(51):25598–25602.
19. Jungwirth P, Tobias DJ (2006) Specific ion effects at the air/water interface. *Chem Rev* 106(4):1259–1281.
20. Hu JH, et al. (1993) Uptake of gas-phase halogenated acetic-acid molecules by water surfaces. *J Phys Chem* 97:11037–11042.
21. Davidovits P, Kolb CE, Williams LR, Jayne JT, Worsnop DR (2006) Mass accommodation and chemical reactions at gas-liquid interfaces. *Chem Rev* 106(4):1323–1354.
22. Enami S, Hoffmann MR, Colussi AJ (2010) Proton availability at the air/water interface. *J Phys Chem Lett* 1:1599–1604.
23. Kathmann SM, Kuo IFW, Mundy CJ, Schenter GK (2011) Understanding the surface potential of water. *J Phys Chem B* 115(15):4369–4377.
24. Healy TW, Fuerstenau DW (2007) The isoelectric point/point-of zero-charge of interfaces formed by aqueous solutions and nonpolar solids, liquids, and gases. *J Colloid Interface Sci* 309(1):183–188.
25. Healy TW, Yates DE, White LR, Chan D (1977) Nernstian and non-Nernstian potential differences at aqueous interfaces. *J Electroanal Chem* 80:57–66.
26. Zhao XL, Ong SW, Eisenthal KB (1993) Polarization of water-molecules at a charged interface—2nd harmonic studies of charged monolayers at the air-water-interface. *Chem Phys Lett* 202:513–520.
27. Luo GM, et al. (2006) Ion distributions near a liquid-liquid interface. *Science* 311 (5758):216–218.
28. Yamaguchi S, Bhattacharyya K, Tahara T (2011) Acid-base equilibrium at an aqueous interface: pH spectrometry by heterodyne-detected electronic sum frequency generation. *J Phys Chem C* 115:4168–4173.
29. Mulkidjanian AY, Heberle J, Cherepanov DA (2006) Protons @ interfaces: Implications for biological energy conversion. *Biochim Biophys Acta Bioenerg* 1757:913–930.

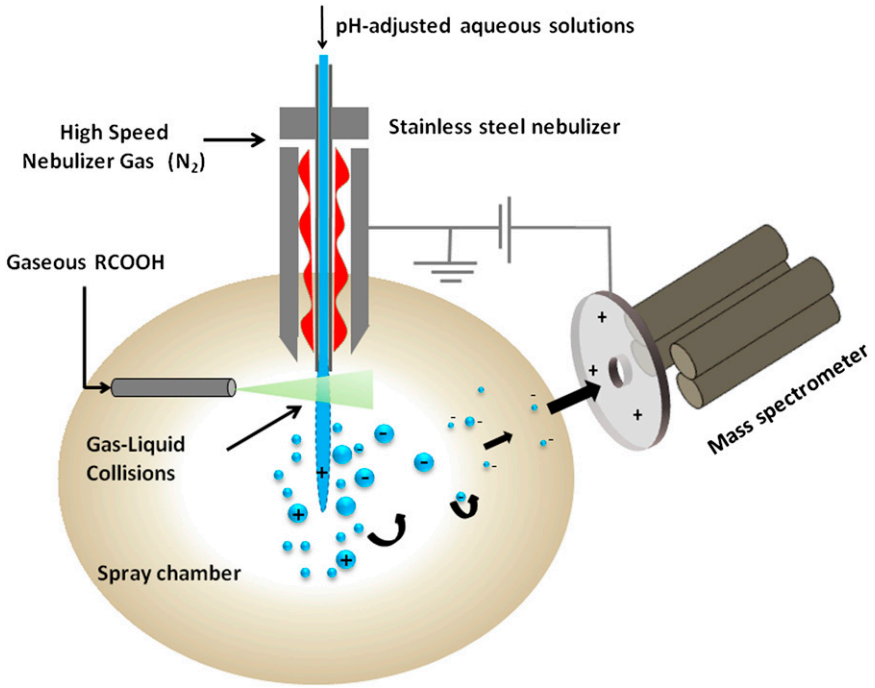

Fig. S1. Schematic diagram of the experimental setup. Aqueous solutions are injected in the spraying chamber (shown in blue) of an electrospray mass spectrometer by through an electrically grounded stainless steel nebulizer (100 μm internal diameter) and briefly exposed to RCOOH(g) (shown in green). Concentric flow of nebulizer gas (shown in red) shears aqueous jet into smaller droplets within ~10 μs, some of which carry excess charge. After subsequent solvent evaporation those charged drops become increasingly unstable due electrostatic repulsion and excess ion(s) are ultimately ejected to the gas phase via field desorption, and detected by mass spectrometry in < 1 ms. The spray chamber is at 1 atm of N_2, 293 K throughout.

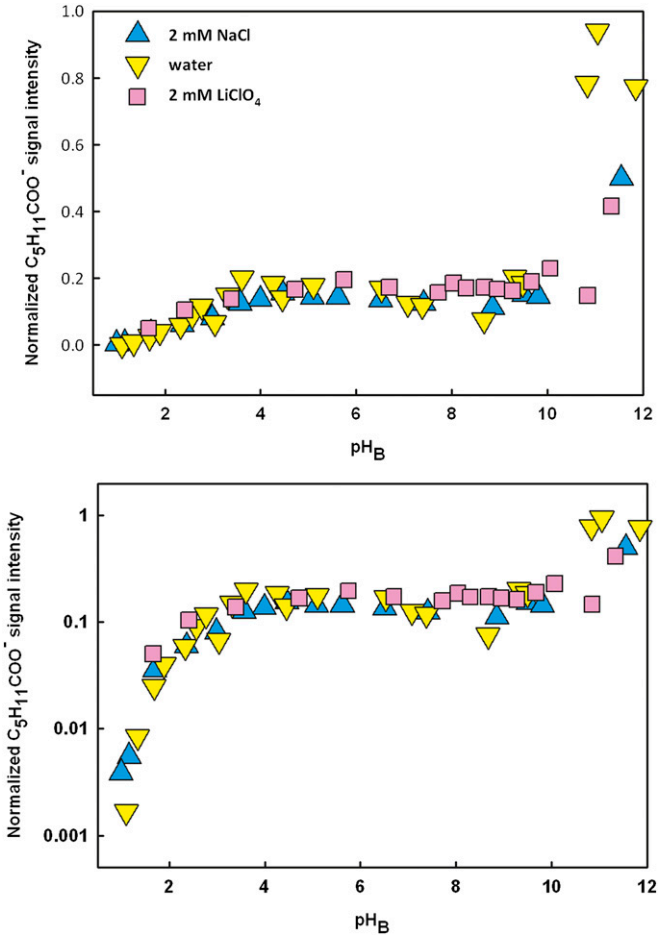

Fig. S2. Dissociation of gaseous hexanoic acid vapors at the air–water interface as a function of the pH of bulk water in the absence and presence of inert electrolytes. Unlike the case of the strong HNO3, interanions are unable to catalyze the dissociation of a weak carboxylic acid. All experiments in 1 atm of N_2 at 293 K.

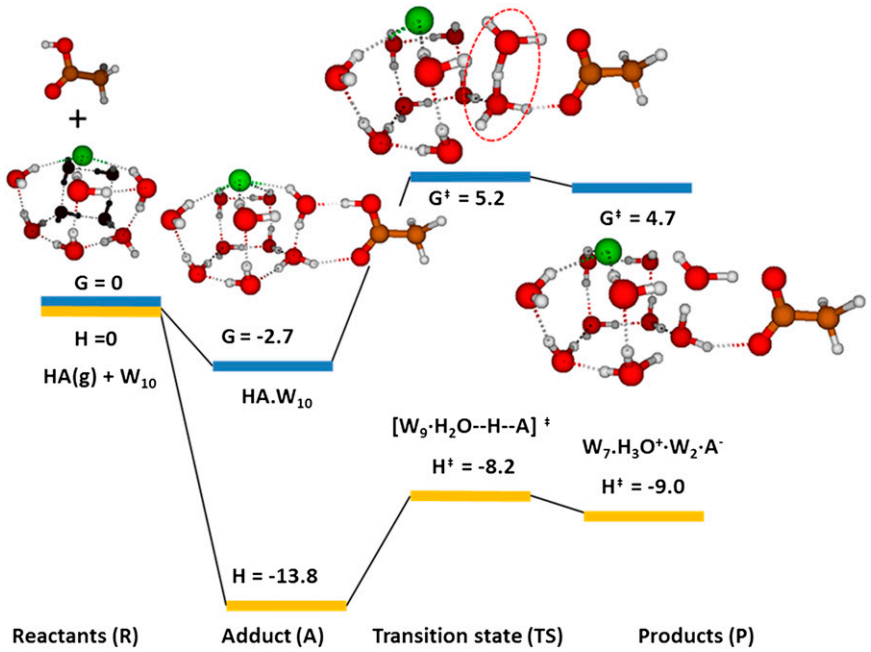

Fig. S3. Lack of chloride (green atom) effects on proton transfer from gaseous CH_3COOH to the surface of water. Unlike the case of HNO_3 (15), chloride is unable to catalyze CH_3COOH dissociation.